JOURNAL OF APPLIED ELECTROCHEMISTRY 9 (1979) 89–100

Negative electrodes for nickel-cadmium accumulators: their properties as determined by impregnation procedure

J. MAREK, I. MOHYLA, J. KOS

Research and Development Laboratories, Bateria Slaný n.p., Czechoslovakia

M. KRČEK

Poldi SONP Kladno, Czechoslovakia

Received 4 April 1978

Sintered negative electrodes for nickel–cadmium secondary cells were studied. Model electrodes prepared by means of three different impregnation methods were evaluated. It was demonstrated that the impregnation procedure may affect properties of active mass and the service life of electrodes in a significant way.

1. Introduction

Considerable attention has been paid to the problems of service life and reliability of sealed Ni–Cd accumulators (see, for example [1–6]), especially in the area of space technology. Many authors have also studied the mechanism of operation of cadmium electrodes in an alkaline electrolyte. Numerous references can be found, for example in reviews [7–9]; important papers include [10–20].

Weininger, Lifshin *et al.* [21, 22] studied cadmium distribution in the plane of a section and found a redistribution during cycling. Choking of pore necks with precipitated $Cd(OH)_2$ was also observed [23, 24]. Armstrong *et al.* [25] compared the behaviour of a porous cadmium electrode with that of a smooth cadmium electrode.

Barnard and co-workers [26] used chemical analysis, cyclic voltammetry, and microscopy for observing the behaviour of porous Cd electrodes during cycling. They found that the amount of Cd metal in discharged electrodes and the amount of $Cd(OH)_2$ in charged electrodes increased with cycle number; further processes took place simultaneously (the active surface area of Cd metal was decreased, Cd and $Cd(OH)_2$ crystallites grew in size, and there was a migration of the active mass towards the outer surface of the electrodes). Thus the lowering of the electrode capacity observed is caused by a decrease in the surface area of Cd metal and blocking of the remaining surface by a relatively non-porous layer of $Cd(OH)_2$. According to these as well as other authors [27] the large crystals formed are not reduced in further cycles and cause a significant decrease in capacity.

Among numerous other papers, we must at least cite the extensive work of Barnard *et al.* [28], who used both light and scanning electron microscopy to study the growth and redistribution of Cd and $Cd(OH)_2$ in sintered plate cadmium electrodes. The dependence of these phenomena upon charge current values and cycle number was monitored. Two types of $Cd(OH)_2$ layers on Cd metal particles were found after discharge. A negative influence of active mass migration towards the electrode surface was also ascertained.

2. The chosen impregnation methods

Since the late twenties, when the patent concerning sintered plate electrodes was published [29], many methods for impregnation of electrodes with electrochemically active cadmium compounds were described. In many cases, how-

ever, these methods represent only minor modifications of fundamental procedures and some of the patents describe methods for preparation of electrodes which are impractical. We have chosen two basic methods for the present research:

(a) impregnation in a solution of cadmium nitrate by a modified Fleischer's method [30],
(b) impregnation in a solution of cadmium formate with subsequent thermal decomposition [31].

It was found during our preliminary studies that electrodes prepared according to (a) attain the highest value of electrochemical efficiency of active mass. Method (b) has other advantages (it is rapid and inexpensive, eliminates lengthy washing, cleaning, and drying operations between individual impregnation cycles, prevents contamination by Ni^{2+} ions, and does not require an inert atmosphere). Fig. 1 gives a dependence of the capacity of model electrodes impregnated by both methods on the number of charging and discharging cycles.

It seems promising to seek a combination of the good properties from both impregnation procedures, i.e., the high coefficient of exploitation of active mass in the case of electrodes impregnated in cadmium nitrate and the shape of the service life curve for electrodes impregnated by means of the formate method. A method found during preliminary experiments involves thermal decomposition of cadmium formate followed by an additional impregnation in cadmium nitrate.

In the course of the present study, we have studied the behaviour of electrodes impregnated by this new method as compared with electrodes impregnated by means of both procedures described earlier. Part of the measurements described here has been published in the form of preliminary communications [32, 33].

3. Experimental

In order to evaluate the properties of model electrodes during their service life, several methods described in the following paragraphs were used.

3.1. *Preparation of model cells*

Circular cadmium electrodes with a diameter of 23 mm were used for all measurements. The pore size distribution of the sintered plate used is given

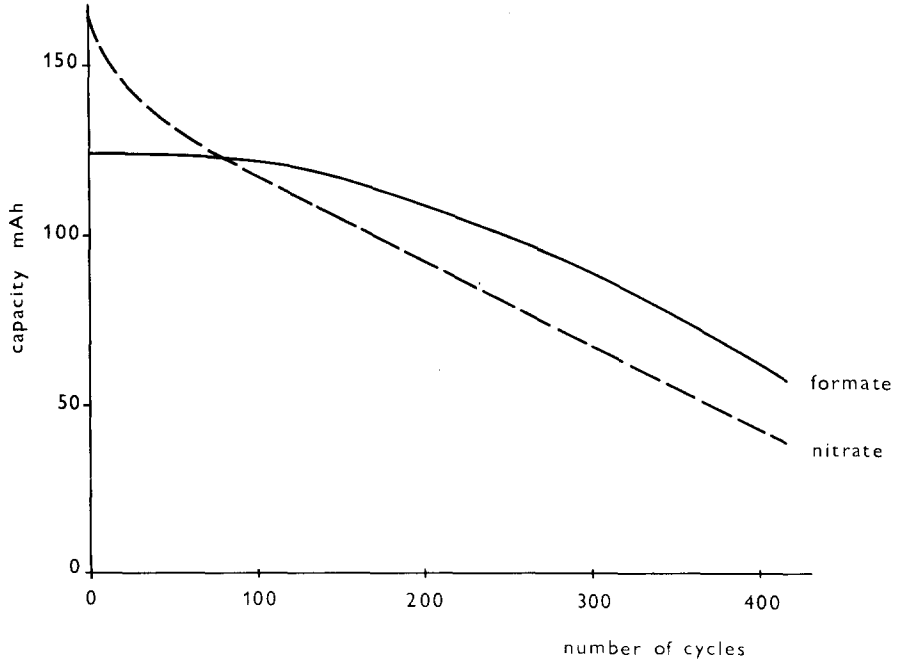

Fig. 1. Service life curves for negative electrode impregnated in cadmium nitrate and formate.

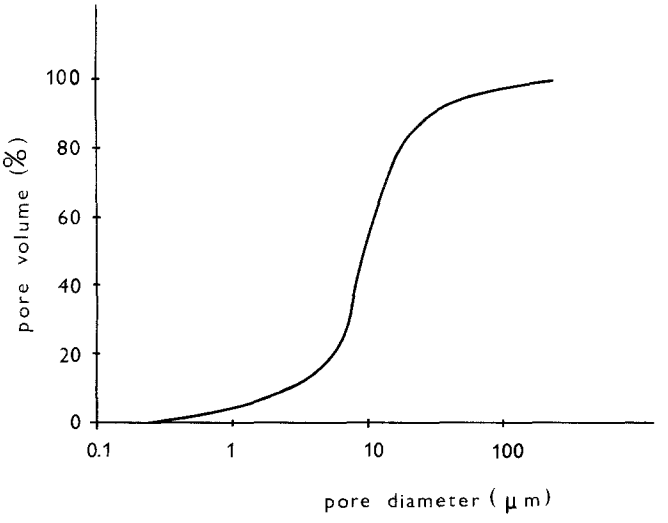

Fig. 2. Integral porosity curve of the sintered plate used.

in Fig. 2; it was measured on a high-pressure mercury porosimeter Carlo Erba 65 H. Before the final measurements, the surface of the plate was coated with a 1% solution of stearic acid in chloroform [34] in order to prevent amalgamation. A positive pocket electrode (600 mA h) served as the counter-electrode. The electrodes were separated from each other by three layers of a non-woven polyamide textile with total thickness 0·45 mm. The cell was constructed in a perspex vessel (electrolyte volume 30 ml). The arrangement of the cell is illustrated in Fig. 3. The temperature during charging and discharging was kept at 21 ± 1° C. In all measurements, a 31% aqueous solution of KOH was used as the electrolyte and Hg/HgO/31% KOH as the reference electrode.

Model electrodes were prepared by the three following impregnation procedures:

(A) Impregnation in a solution of cadmium formate with subsequent thermal decomposition (5 cycles) (see [31]).
(B) Impregnation in a solution of cadmium nitrate (5 cycles) according to a modified version of the Fleischer process [30].
(C) 4 cycles according to (A) + an additional impregnation according to (B).

In the following paragraphs, the electrodes measured are denoted as model Electrodes A, B and C, accordingly. Only Electrodes A–C containing 0·278 ± 0·005 g Cd were used. In the case of Electrodes C, the additionally impregnated

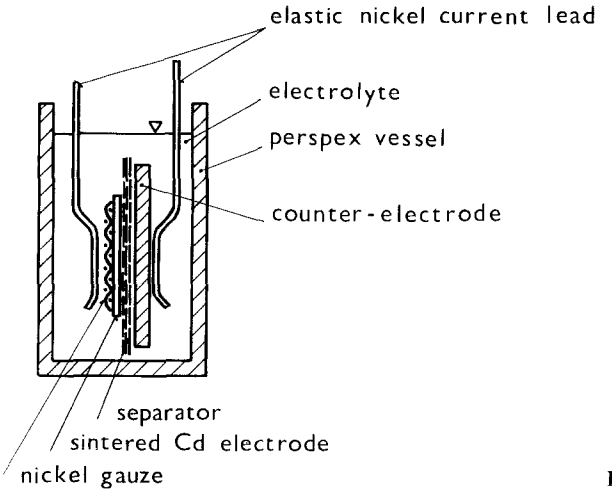

Fig. 3. Arrangement of the model cell.

active mass represents about 17% of the total Cd content.

3.2. *Measurements of electrode capacity and service life characteristics*

During the first charging cycle, the electrode was formed by a 80 mA current for 16 hours with subsequent discharge by a current of 60 mA to −650 mV against the reference electrode. The second cycle comprised charging at 200 mA for one hour. Afterwards, automatic cycling equipment was switched on with the following operating mode: discharge by 390 mA for 8 min (52 mA h), 1 min pause, charge by 200 mA for 20 min (66·7 mA h). In every 35th–40th cycle (or, if need be, earlier), the automatic apparatus was switched off after completion of charging and a capacity measurement was performed according to the procedure used in the first cycle. Subsequent to charging by 200 mA for one hour, automatic cycling was continued.

3.3. *Chemical analysis*

In order to perform quantitative parallel determinations of Cd and Cd^{2+}, the gasometric method of Barnard *et al.* [26] was used. Cd metal was determined quantitatively by measuring the volume of hydrogen developed from the electrode in a 1 M CH_3COOH and 1 M CH_3COONa solution. The total amount of Cd was determined by complexometry.

3.4. *Scanning electron microscopy and X-ray microanalysis*

A scanning electron microscope JEOL JSM-U3 was used and an energy dispersive X-ray microanalyzer EDAX.

A secondary electron image at an accelerating voltage of 25 kV was used for microscopic observations. A method previously described [33] was exploited for observing identical regions on the electrode surface during the cycling process.

The large depth of focus of the scanning electron microscope enabled us to monitor also the changes taking place on electrode fractures during cycling. Observing an identical region was naturally impossible here and thus the samples were stuck to the specimen holder with a conductive glue and a C/Au layer was evaporated onto them. By moving in the direction perpendicular to the electrode surface, continuous strips of micrographs corresponding to the total width of the fraction were obtained, always in that part of the fracture where the nickel sheet was perforated.

Samples for microscopic observations were prepared by discharging the electrodes to 200 mV against the reference electrode, washing in water until the reaction with phenolphthalein vanished and for a further hour, and drying for 2 hours in a stream of nitrogen at 80° C.

X-ray microanalysis was used for: surface analyses of electrodes; identification of individual particles on secondary electron images (lines used: Cd $L\alpha_1$ 3·133 keV, Ni $K\alpha$ 7·471 keV); and monitoring the active mass distribution in electrodes by measurements of the intensity distribution of the Cd $L\alpha_1$ signal in the plane of a metallographic specimen perpendicular to the electrode surface. This polished section was prepared after impregnating the electrode with an epoxide resin.

3.5. *Specific surface area measurements*

The specific surface area was determined by a modified BET method on a Perkin–Elmer 212D Sorptometer. Helium served as the carrier gas and N_2 as adsorbate. The samples were activated by heating them to 60° C in a flow of He for one hour. The specific surface area was related to the amount of active mass present. In the case of the sintered plate, this value was verified also by means of stereology (see, for example [35–37]). Sample preparation procedure was the same as for electron microscopy (see Section 3.4).

3.6. *Measurements of free pore volume*

The free volume of pores communicating with the surface was measured by filling them with water. The sample immersed in water was put into a vessel and the pressure was lowered to the boiling point of water. After one minute the pressure was equalized with the atmospheric pressure, remaining drops of water were wiped off the surface, the sample was weighed and the volume of water was related to the geometrical volume of the porous layer in question.

3.7. *I–t curves at constant potential*

Measurements were carried out at a potential of −1050 mV against the reference electrode. The instruments used were a Pie 06 Svuom potentiostat, a millivoltmeter–picoammeter BM 483, and a strip chart recorder. The cell was made of perspex and the tip of the Luggin capillary (0·5 mm in diameter) was placed very near to the electrode. The counter-electrode was made of pure Ni, and the working electrode had an area of 1 cm^2.

4. Results and discussion

The dependence of electrode capacity on the length of the formation period is given in Fig. 4. A similar result was obtained from measurements of *I–t* curves; it is evident that there is a big difference in the reducibility of active mass for Electrodes A–C. The next important part of our results can be deduced from the capacity decrease during cycling (Fig. 5), namely that from approximately the 100th cycle onwards Electrodes C are characterized by the highest values of capacity. The curve of the specific surface area versus the cycle number (Fig. 6) suggests there is (*inter alia*) an activation of the surface of CdO originally present, because the increase in specific surface area of Electrodes C as compared with Electrodes A is higher than might be otherwise supposed. Fig. 7 is an illustration of changes in free pore volume during the service life. Porosity is increased in all cases with increasing cycle number and the different starting values becoming nearly equal after 400 cycles. However, the increase in the case of Electrodes B is the steepest. Results of chemical analyses are summarized in Fig. 8. Conditions of 'charge' and 'discharge' here correspond to the conditions of the service life test previously described. An important result of these measurements is the fact that the decrease in the efficiency of utilization of the active mass for Electrodes B is caused predominantly by a poorer oxidizability of Cd metal particles.

When identifying main components on micrographs, their characteristic shape served as a useful criterion, verified by X-ray microanalysis. The shape of the nickel sinter is quite characteristic and can be clearly seen, e.g. on Fig. 11(d) in contrast to the $Cd(OH)_2$ crystals. Four regions were randomly chosen on each electrode (on both sides with respect to the counter-electrode) for the final

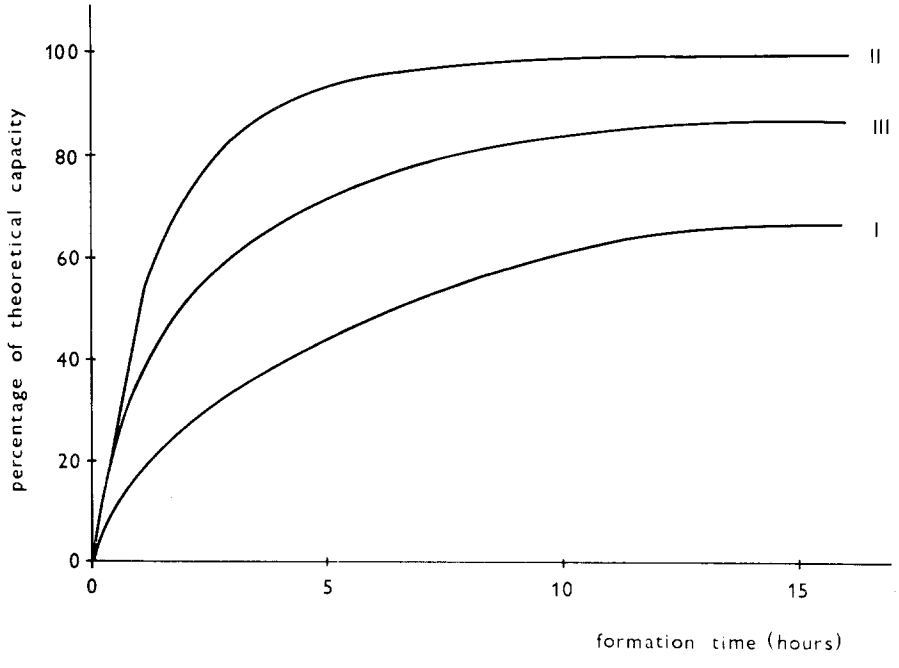

Fig. 4. Dependence of electrode capacity in the first discharge cycle on the time of formation.

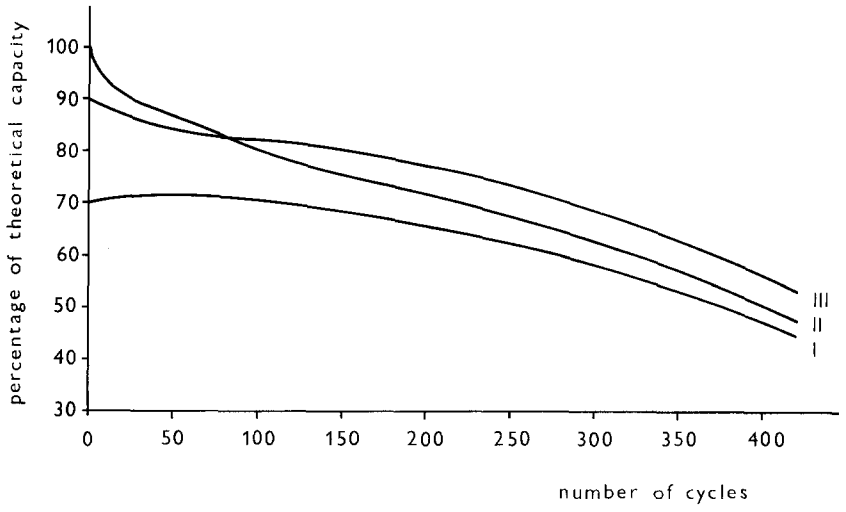

Fig. 5. Dependence of electrode capacity on the number of charge and discharge cycles.

microscopic examination of changes on the electrode surface, in order to guarantee a sufficient degree of reproducibility of phenomena observed. The areas selected were photographed many times during the whole service life (i.e. sintered plates, impregnated electrodes, and electrodes after various numbers of cycles), always at three magnifications, which were found to yield the most information (300, 1000, 3000). No observable differences were found between micrographs of charged and discharged electrodes at the same cycle number. With regard to experimental difficulties encountered when manipulating charged electrodes, micrographs of discharged electrodes were taken throughout. Another interesting discovery was the fact that there is no substantial difference between the character of the surface facing the counter-electrode and that of the surface on the opposite side. Because of the large amount of photographic material obtained during these measurements, only a very abbreviated series per electrode type will be presented here. The numbers

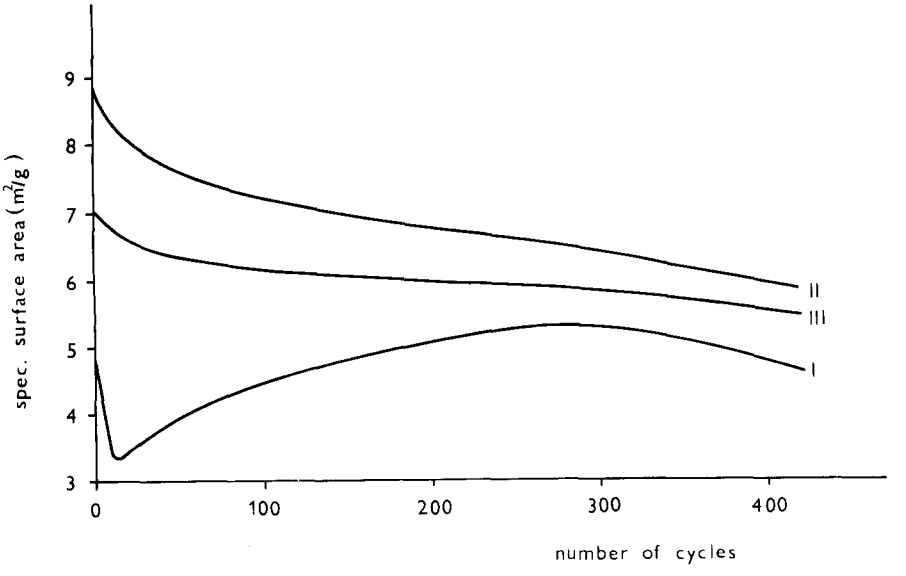

Fig. 6. Changes in specific surface area of electrodes during cycling.

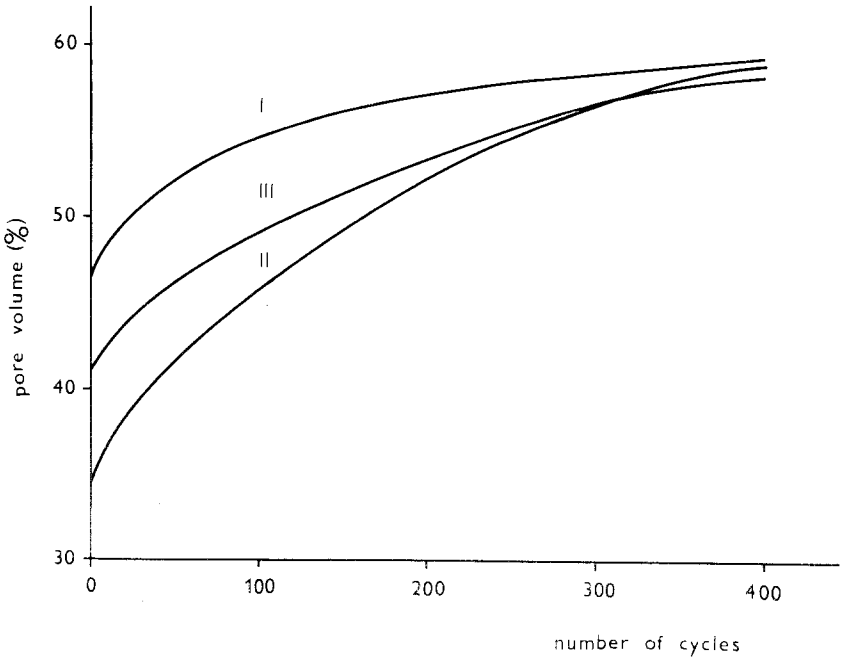

Fig. 7. Dependence of free pore volume on cycle number.

of cycles corresponding to the presented micrographs were chosen so as to stress the characteristic course of changes on the electrode surface.

The surface of Electrode A during cycling is shown in Fig. 9(a)–(d). The original finely-divided active mass is being replaced with crystals approxi-

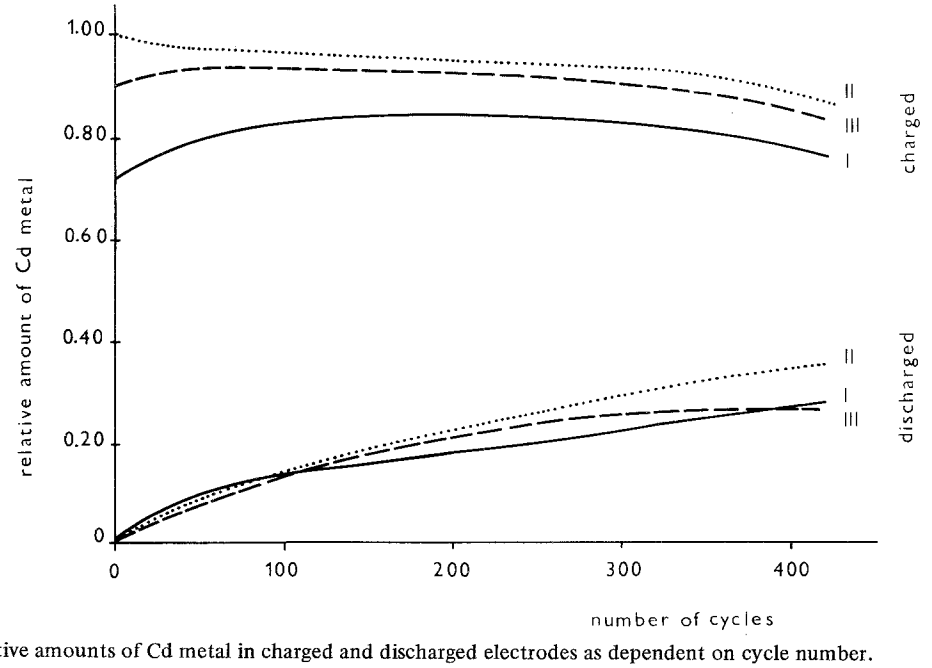

Fig. 8. Relative amounts of Cd metal in charged and discharged electrodes as dependent on cycle number.

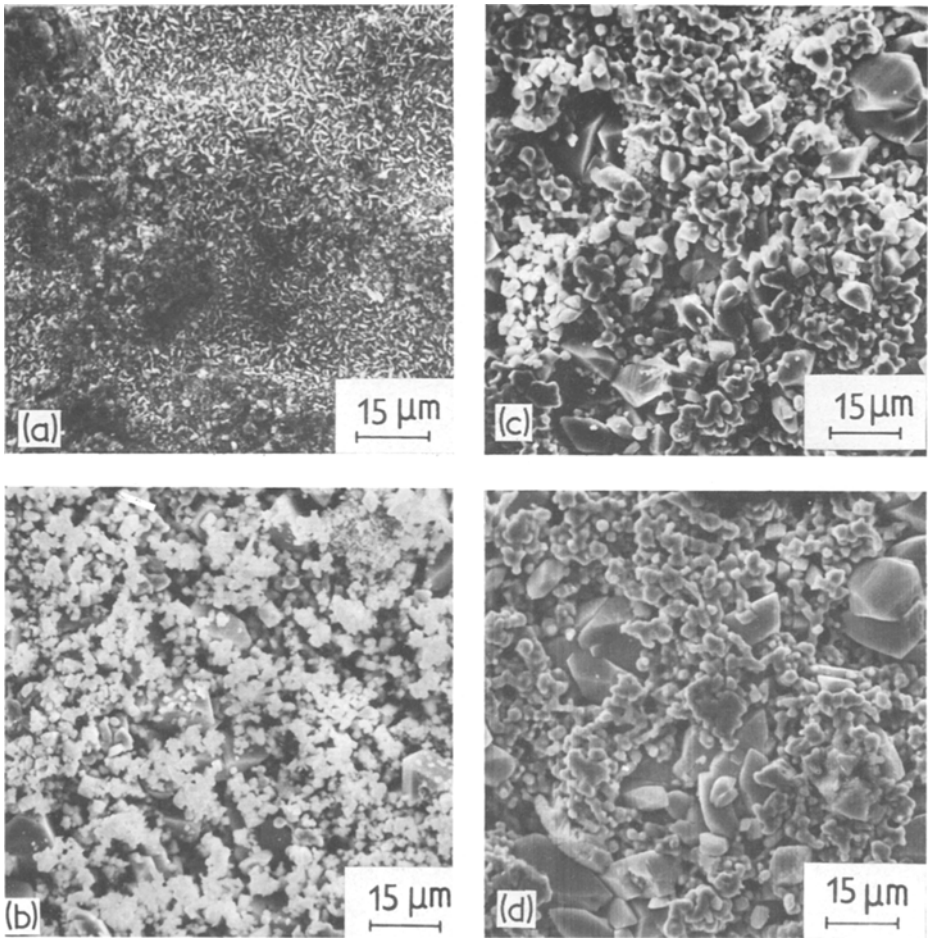

Fig. 9. Electrode A after: (a) 1 cycle, (b) 41 cycles, (c) 62 cycles, (d) 112 cycles.

mately 10 times larger, which in turn are growing during further cycling.

The changes in Electrode B are presented in Fig. 10. Larger crystals can be found here only after the 5th cycle and even during following cycles, when the surface of the sintered plate becomes visible, large β-$Cd(OH)_2$ crystals are found only rarely. Etching effects can be found on the stripped part of the sintered plate, caused by the nitrate impregnation bath, but only at higher magnifications than that of Fig. 10.

Fig. 11 represents the results with an electrode of type C. Morphological changes are similar to those for Electrode B, only the etching effects are less pronounced.

For all electrode types investigated, detachment of crystals was observed, especially for crystals formed on the surface with the exception of those in the mouths of larger pores. This fact can be accounted for by the influence of manipulation (washing, drying). Published micrographs [33] may be used here for a demonstration of this effect. At a certain stage of cycling, the crystals in the mouths to the pore are also lost and simultaneously etching of some crystals protruding from the sintered plate surface was observed. It can be concluded that for the given conditions (cycling in excess electrolyte) even relatively large crystals are being dissolved. This phenomenon is characteristic, however, only of the surface layer exposed to convection of the electrolyte, while in deeper layers a monotonic growth of crystals was observed.

We are well aware that the conditions in these

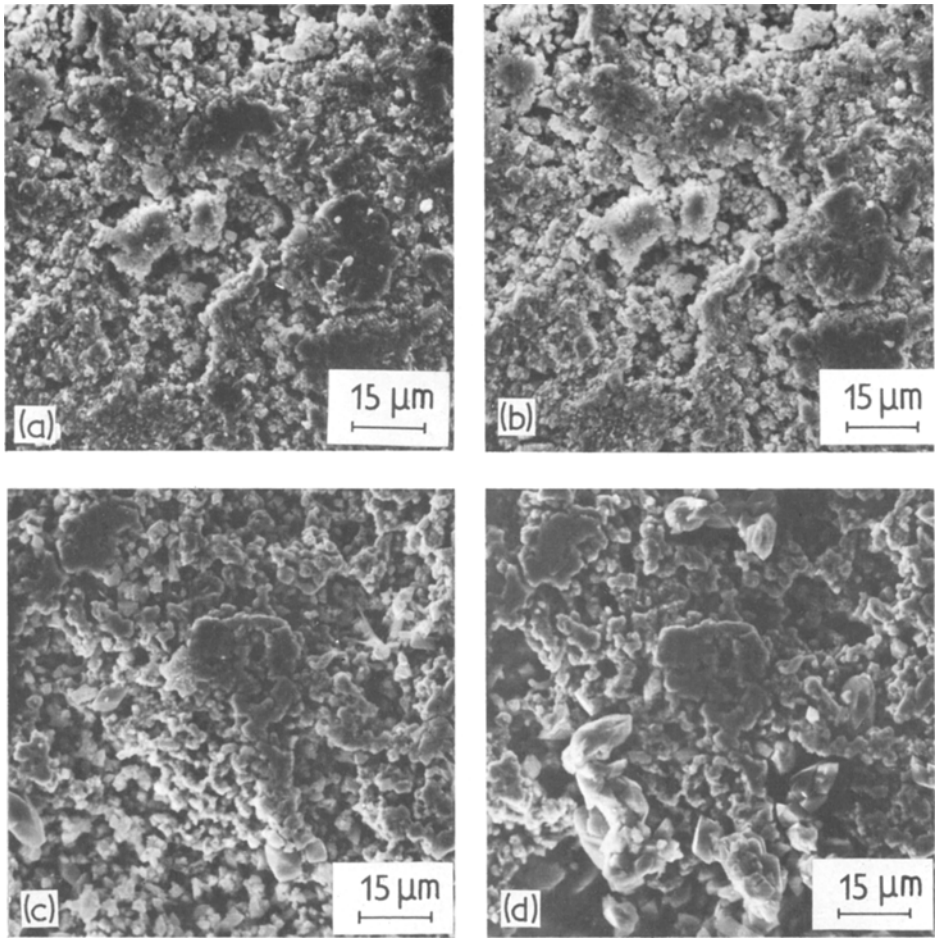

Fig. 10. Electrode B after: (a) 5 cycles, (b) 41 cycles, (c) 250 cycles, (d) 419 cycles.

experiments only approximate poorly to those in a real sealed accumulator. Fig. 12 is an example of the surface of an electrode taken from a sealed accumulator after 250 deep discharge and charge cycles carried out in the temperature range 0–55°C. It is evident that the total electrode surface is covered with $Cd(OH)_2$ crystals under these conditions.

Micrographs of electrode fractures cannot be published here because of the length of the paper. The use of fractures has several advantages as compared with the commonly used technique of metallographic specimens, namely, an easier identification of particles and an easier specimen preparation. Our results indicate that even after large numbers of cycles, the layer of active mass with large crystals is limited to a small part of the electrode facing the counter-electrode. The largest crystal growth was found for Electrodes A; no significant difference was determined between Electrodes B and C.

For X-ray investigations of active mass migration, electrode fractures were useless and the measurements were realized on polished sections. Significant accumulation of Cd in surface layers was observed only for Electrodes B (see Fig. 13 and Section 3.4), in the case of Electrodes A and C these effects are substantially less pronounced. However, in all cases investigated this accumulation was found in those areas of the sintered plate which contained extremely large pores or cracks.

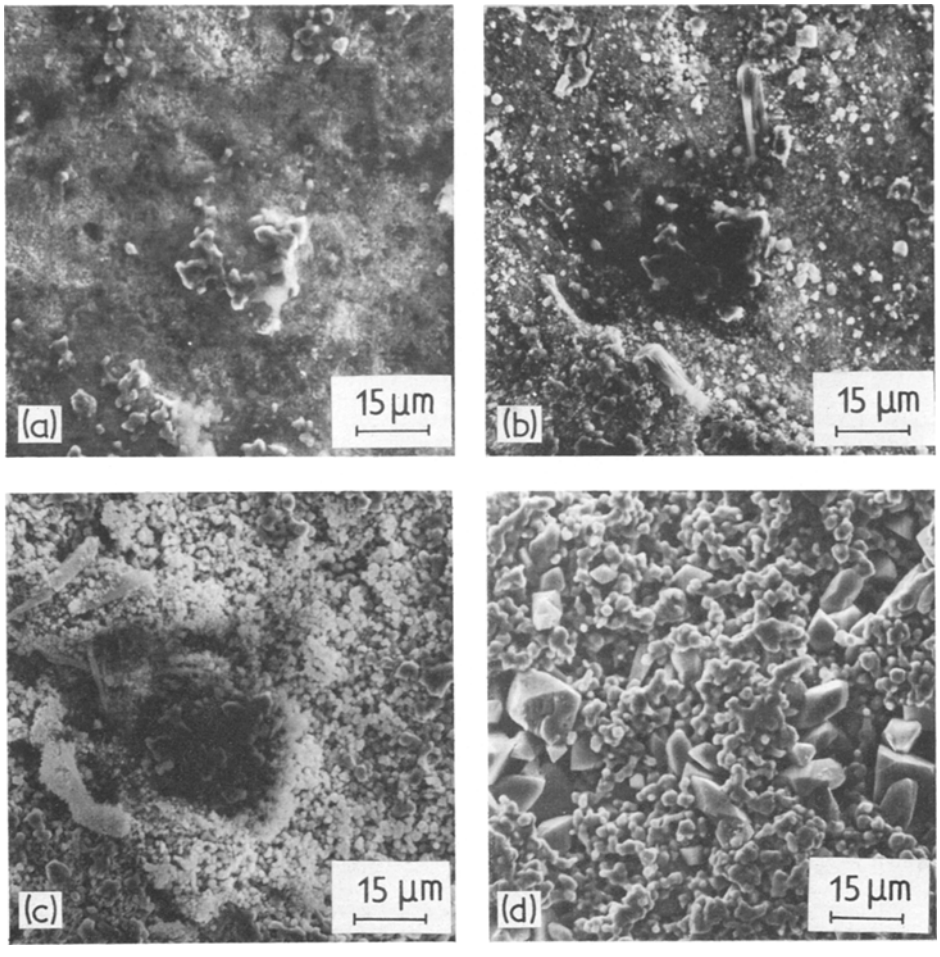

Fig. 11. Electrode C after: (a) impregnation, (b) 5 cycles, (c) 62 cycles, (d) 419 cycles.

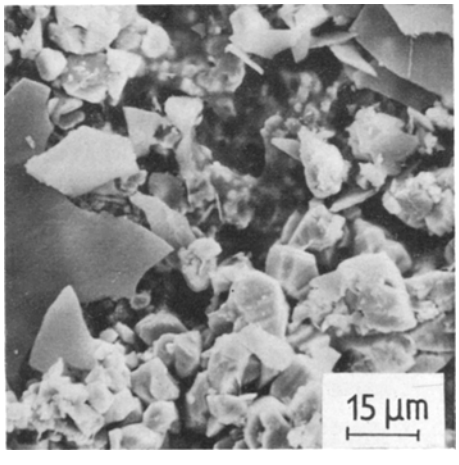

Fig. 12. Surface of an electrode from a sealed accumulator, 250 cycles.

5. Conclusions

The following conclusions were reached:

(a) The capacity and service life of these sintered plates depend on the active mass, which in turn is determined largely by the impregnation method.

(b) The reducibility of the active mass of Electrodes A was poor. This may be caused by the presence of larger particles (lower specific surface area), and/or by an insufficient electrical contact among particles. The latter effect can be substantiated by a certain amount of CdO falling from the pores during mechanical manipulations with these electrodes.

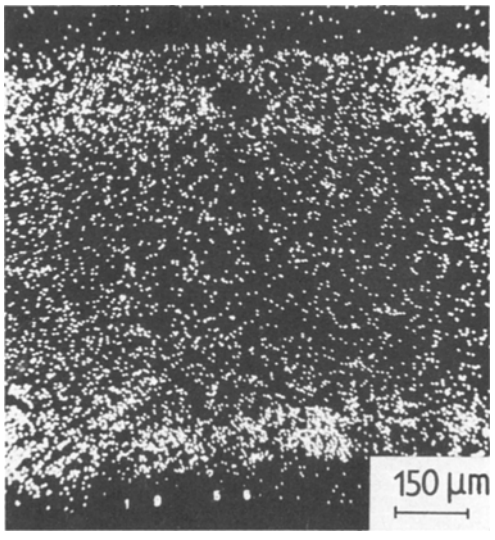

Fig. 13. Relative frequency of the Cd $L\alpha_1$ signal in the plane of the metallographic specimen. Electrode B, 419 cycles, counter-electrode downwards.

(c) In the case of Electrodes B and C, the remaining unreduced fine precipitate of $Cd(OH)_2$ represents a large number of crystallization centres and promotes formation of small $Cd(OH)_2$ crystals. Large crystals in the case of Electrodes A cause a decrease in charging efficiency.

(d) The amount of Cd metal in the discharged electrodes is originally identical, but towards the end of the service life it is higher for Electrodes B. This fact may be caused by a higher nickel content in the active mass and by a high accumulation of active mass in surface layers.

(e) Higher efficiency of the active mass was found for electrodes with higher values of specific surface area; however, no direct relationship exists between these two quantities.

(f) Morphological changes taking place during cycling are affected mainly by dissolution and crystallization processes. This fact, however, does not rule out contributions by solid-state routes in electrode processes.

(g) No observable losses of Cd from the electrodes were found. A negligible mass loss in discharged electrodes during cycling corresponds to the growing amount of Cd metal.

(h) Better efficiency of the active mass of Electrodes C as compared with Electrodes A during the whole service life is caused by a higher charging efficiency.

(i) The additional impregnation in a $Cd(NO_3)_2 \cdot 4H_2O$ melt results in a significant increase in specific surface area of the active mass. A part of the CdO is dissolved in the nitrate bath and again precipitates as $Cd(OH)_2$, the surface of other CdO particles is probably etched. The presence of the $Cd(OH)_2$ precipitate results also in a better electronic conductivity.

(j) Electrodes C have the following advantages as compared with Electrodes B: a lower content of Cd metal after discharge, a lower rate of corrosion of the sintered plate and thus a lower contamination of the active mass by nickel, and lower accumulation of active mass mass in surface layers.

References

[1] Report NASA N 69 13454, CR 97 935 (1968).
[2] Report NASA N 70 12 539, CR 107 119 (1969).
[3] Report NASA N 70 35 744, NAS 5 11 547 (1970).
[4] Report ESRO TM 138 (ESTEC) (1969).
[5] F. Putois, *Rev. Gén. Elect.* **84** (1975) 473.
[6] S. Gross, *Energy Conv.* **11** (1971) 39.
[7] R. D. Armstrong, K. Edmonson and G. D. West, 'Specialist Periodical Reports, Electrochemistry', Vol. 4, The Chemical Society, London (1974) p. 18.
[8] S. U. Falk and A. J. Salkind, 'Alkaline Storage Batteries', J. Wiley (1969).
[9] J. Marek, Thesis, FE VUT Brno (1977).
[10] J. S. Newman and C. W. Tobias, *J. Electrochem. Soc.* **109** (1962) 1183.
[11] E. A. Grens, *Electrochim. Acta* **15** (1970) 1047.
[12] R. C. Alkire, E. A. Grens and C. W. Tobias, *J. Electrochem. Soc.* **116** (1969) 1328.
[13] K. Micka, *Coll. Czech. Chem. Commun.* **29** (1964) 1998.
[14] J. D. Zitner, E. A. Maksimyuk, V. A. Nikolskii, N. I. Alekseyeva and E. A. Berkman, *Elektrokhim.* 7 (1971) 1581.
[15] J. S. Dunning, D. N. Bennion and J. Newman, *J. Electrochem. Soc.* **120** (1973) 906.
[16] P. Selanger, *J. Appl. Electrochem.* 4 (1974) 249, 259, 263.
[17] J. P. Harivel, B. Morignat and J. Migeon, 'Batteries 2', *Proceedings 4th International Symposium*, Brighton (1964) Pergamon Press (1965) p. 107.
[18] M. H. Gottlieb, *Electrochem. Technol.* **5** (1967) 12.
[19] Y. Okinaka and C. M. Whitehurst, *J. Electrochem. Soc.* **117** (1970) 538.
[20] A. J. Salkind, H. J. Canning and M. L. Block, *Electrochem. Technol.* 2 (1964) 254.

[21] J. L. Weininger and M. W. Breiter, 'Power Sources', *Proceedings 5th International Symposium*, Brighton (1966) Pergamon Press (1967) p. 269.
[22] E. Lifshin and J. L. Weininger, *Electrochem. Technol.* **5** (1967) 5.
[23] E. J. Casey and J. B. Vergette, *Electrochim. Acta* **14** (1969) 697.
[24] P. Bro and H. Y. Kang, *J. Electrochem. Soc.* **118** (1971) 519.
[25] R. D. Armstrong, A. D. Sperin, F. L. Tye and G. D. West, *J. Appl. Electrochem.* **2** (1972) 265.
[26] R. Barnard, J. A. Lee, A. H. Rafinski and F. L. Tye, 'Power Sources 5', *Proceedings 9th International Symposium*, Brighton (1974) p. 183.
[27] F. G. Will and H. J. Hess, *J. Electrochem. Soc.* **120** (1973) 1.
[28] R. Barnard, G. S. Edwards, J. A. Lee and F. L. Tye, *J. Appl. Electrochem.* **6** (1976) 431.
[29] German patent 491 498.
[30] A. Fleischer, *J. Electrochem. Soc.* **94** (1948) 289.
[31] Swedish patent 227 535.
[32] J. Marek, I. Mohyla and M. Stompfe, *28th Meeting of ISE, Extended Abstracts II*, 397, Varna (1977).
[33] I. Mohyla and J. Marek, *J. Appl. Electrochem.* **8** (1978) 365.
[34] M. Svatá, in 'Porosimetry and Its Applications', (ed. S. Modrý), Czech. Sci. Techn. Soc., Prague (1969) pp. 94–121.
[35] Z. Ministr, *Pract. Metall.* **12** (1975) 244.
[36] Z. Ministr, I. Mohyla and J. Marek, *Powder Metall. Intern.* **10** (1978) 21.
[37] Z. Ministr and I. Mohyla, *Colloquium on the Applications of Stereology and Computing*, Vys. Tatry, Proc. (1976) p. 213.